

Programming shape using kirigami tessellations

Gary P. T. Choi¹, Levi H. Dudte¹ and L. Mahadevan^{1,2,3*}

Kirigami tessellations, regular planar patterns formed by partially cutting flat, thin sheets, allow compact shapes to morph into open structures with rich geometries and unusual material properties. However, geometric and topological constraints make the design of such structures challenging. Here we pose and solve the inverse problem of determining the number, size and orientation of cuts that enables the deployment of a closed, compact regular kirigami tessellation to conform approximately to any prescribed target shape in two or three dimensions. We first identify the constraints on the lengths and angles of generalized kirigami tessellations that guarantee that their reconfigured face geometries can be contracted from a non-trivial deployed shape to a compact, non-overlapping planar cut pattern. We then encode these conditions into a flexible constrained optimization framework to obtain generalized kirigami patterns derived from various periodic tessellations of the plane that can be deployed into a wide variety of prescribed shapes. A simple mechanical analysis of the resulting structure allows us to determine and control the stability of the deployed state and control the deployment path. Finally, we fabricate physical models that deploy in two and three dimensions to validate this inverse design approach. Altogether, our approach, combining geometry, topology and optimization, highlights the potential for generalized kirigami tessellations as building blocks for shape-morphing mechanical metamaterials.

Kirigami, the creative art of paper cutting and folding, and the tessellations derived from it have recently emerged as prototypical routes towards a new class of mechanical metamaterials. Indeed, various studies have focused on quantifying the geometry and kinematics of deployment of a given kirigami pattern, and their potential as auxetic structures and shape-morphing sheets^{1–18}, the so-called forward problem. From a mathematical, physical and a technological perspective, perhaps an even more interesting question is the inverse problem: can one design the kirigami tessellations in a closed, compact subset of the plane, so that it can be deployed into a prescribed final shape in two or three dimensions? Here, we pose this puzzle as a constrained optimization problem and solve it in a range of situations.

The simplest planar deployable kirigami patterns are based on periodic tilings of the plane using triangles, squares and hexagons, although other complex tessellations inspired by art and architecture have been explored recently^{4,19}. Here we focus on using the quadrilateral kirigami pattern for ease of exposition; however, our methods generalize to any periodic pattern (see Supplementary Information, Section 1). In Fig. 1a, we show the quad tessellation of the plane in its compact and deployed state, with the cuts along the edges of the quads designed to allow for rotational in-plane deployment about a set of hinges. This pattern constitutes a one-degree-of-freedom mechanism whose planar deployment yields a continuous family of self-similar shapes that terminates at self-intersecting configurations. The basic unit cell underlying this pattern is also shown in Fig. 1a in both its undeformed and deformed states and shows the mathematical constraints that define the system: pairs of deployed edges contract to the same edge in the undeformed state, and simultaneously sets of deployed angles contract to the same single vertex in the undeformed state. Given an initially periodic tiling of a patch of the plane with this unit cell, we can state our inverse design problem thus (as shown in Fig. 1b): how should the unit cell be modulated in space to approximate a given planar shape in its deployed

state and still be able to tile a patch of the Euclidean plane compactly when undeformed?

To find a solution requires us to search for potentially admissible results in the deployed space. A first step in this process is to quantify the constraints that will allow the deployed initialization geometry to correspond to a valid kirigami pattern that can compactly close onto a Euclidean patch. The necessary and sufficient contractibility conditions imply that a valid deployed configuration must be able to contract (undeploy) the configuration into a generalized kirigami pattern that closes consistently along the cuts without any mismatch or overlap in lengths and angles. As illustrated in Fig. 1b, the contractibility constraints are: (1) every pair of edges with edge lengths a , b in the deployed space that correspond to the same cut must satisfy the condition

$$a^2 - b^2 = 0 \quad (1)$$

(2) Every set of four angles in the deployed space that correspond to an interior node must sum to 2π , so that

$$\theta_1 + \theta_2 + \theta_3 + \theta_4 = 2\pi \quad (2)$$

where θ_i are angles in the deployed space as illustrated in Fig. 1a (see Supplementary Information, Section 2 for the analogous formulation for other kirigami tessellations).

To be able to deploy a kirigami pattern to match a given shape, we also need to ensure that for a given boundary curve ∂S we have a valid deployed configuration. This can be formulated as boundary-shape matching constraints that force all nodes on the boundary of the deployed configuration to lie exactly on ∂S . Mathematically, for every boundary node \mathbf{p}_i , this implies that

$$\|\mathbf{p}_i - \tilde{\mathbf{p}}_i\|^2 = 0 \quad (3)$$

¹John A. Paulson School of Engineering and Applied Sciences, Harvard University, Cambridge, MA, USA. ²Departments of Physics, and Organismic and Evolutionary Biology, Harvard University, Cambridge, MA, USA. ³Kavli Institute for Nanobio Science and Technology, Harvard University, Cambridge, MA, USA. *e-mail: lmahadev@g.harvard.edu

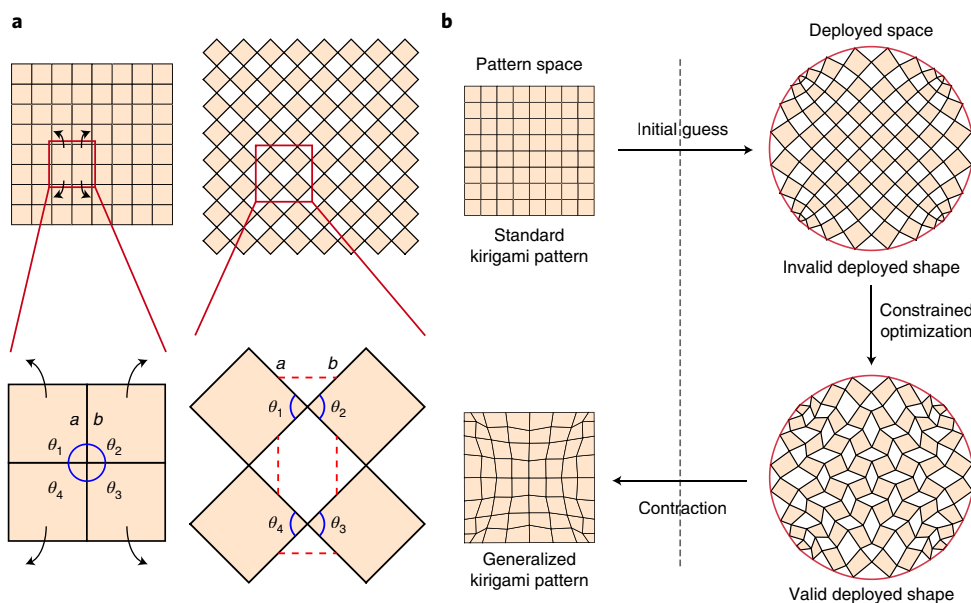


Fig. 1 | Inverse design framework. **a**, A quad kirigami tessellation and its deployed configuration, with an enlargement of the unit cell of the quad kirigami tessellation and its deployed configuration. Every pair of corresponding edges are connected by a red dashed line. The set of angles corresponding to the same node are highlighted in blue. In a valid deployed configuration of a generalized kirigami pattern, every pair of edges should be equal in length, that is $a = b$, and every set of corresponding angles should add up to 2π , that is, $\theta_1 + \theta_2 + \theta_3 + \theta_4 = 2\pi$. **b**, Our inverse design framework. Given a standard kirigami tessellation, we start with an initial guess in the deployed space. Here the initial guess shown is a conformal map from the standard deployed configuration to the disc. The initial guess is usually invalid, violating either the edge length constraint or the angle constraint, or not exactly matching the target boundary shape. We then solve a constrained optimization problem to morph the initial guess until it becomes a valid deployed shape, satisfying all constraints. Finally, we use a simple contraction procedure to obtain the generalized kirigami pattern.

where $\tilde{\mathbf{p}}_i$ is the projection of \mathbf{p}_i onto ∂S and $\|\cdot\|$ is the Euclidean 2-norm. In addition to matching the target boundary shape in the deployed configuration, we can also control the shape of the kirigami tessellations in their undeformed states by introducing boundary angle constraints (see Supplementary Information, Section 2 for details).

While the constraints described above ensure consistency between corresponding edges and angles, they do not prevent the faces from overlapping in the deployed state. To enforce this, we use the following non-overlapping constraint at every angle between two adjacent faces:

$$\langle (\mathbf{b} - \mathbf{a}) \times (\mathbf{c} - \mathbf{a}), \hat{\mathbf{n}} \rangle \geq 0 \quad (4)$$

where \mathbf{a} , \mathbf{b} and \mathbf{c} are the nodes of adjacent faces, so that $(\mathbf{b}, \mathbf{a}, \mathbf{c})$ forms a positive (right-hand ordered) angle between the two faces, and $\hat{\mathbf{n}} = (0, 0, 1)$ is the outward unit normal.

To find an admissible deployed kirigami structure, we must satisfy the above interior and boundary conditions—this will yield a compact tiling that is related to the deployed state via a non-affine contraction. This can be framed as a constrained optimization problem whose solution is sufficient to guarantee a valid deployed configuration of a generalized kirigami pattern that approximates a prescribed shape. However, without a regularization procedure, the solution is likely to be very rough with large gradients in the shapes of the quads. To produce a smooth kirigami tessellation, we therefore minimize the following objective function:

$$\frac{1}{M} \sum_{i=1}^M \left(\sum_j (\alpha_{ij} - \beta_{ij})^2 + \sum_k (a_{ik} - b_{ik})^2 \right) \quad (5)$$

where α_{ij}, β_{ij} are a pair of corresponding angles in two adjacent cells and a_{ik}, b_{ik} are the corresponding edge lengths in two adjacent cells,

and M is the total number of pairs of adjacent cells, subject to the constraints (1)–(4).

Finally, we need a reasonable first approximation to the given deployed configuration that matches the prescribed boundary curve. This initial condition can be obtained via, for example, a conformal/quasi-conformal map^{20,21}, although we could use any approximation that preserves the number and connectedness of the quads.

We solve the optimization problem numerically using MATLAB's built-in optimization routine *fmincon* (see Supplementary Information, Section 3), noting that the problem is underconstrained with multiple admissible deployed kirigami patterns (see Supplementary Information, Sections 2 and 4). Once we find a valid deployed structure, we can contract this into its compact pattern form by rotating the faces and thus shrinking the entire structure. We note here that our formulation of the optimization problem shows some algorithmic similarities to our recent study of generalized origami tessellations²². This is both natural and inevitable, given the presence of geometrical constraints in both problems as well as a condition of shape matching; indeed, many problems in physical geometry requiring the ability to design shapes subject to constraints will also fall within this framework.

To illustrate the effectiveness of our approach, we first design generalized kirigami patterns to approximately solve an ancient mathematical problem—that of circling the square—and a modern one, making an egg shape from a square. In Fig. 2a, we show that by distorting a periodic kirigami tiling of a square (see Supplementary Information), the deployed configurations can match either a circle or an egg. We can also use this method to generate novel generalized kirigami patterns that, when deployed, approximate different boundary shapes. Figure 2b shows two generalized kirigami patterns; one deployed to approximate a domain with a boundary of mixed curvature, and the other deployed to approximate a rectangle (see Supplementary Information, Section 4 for more generalized

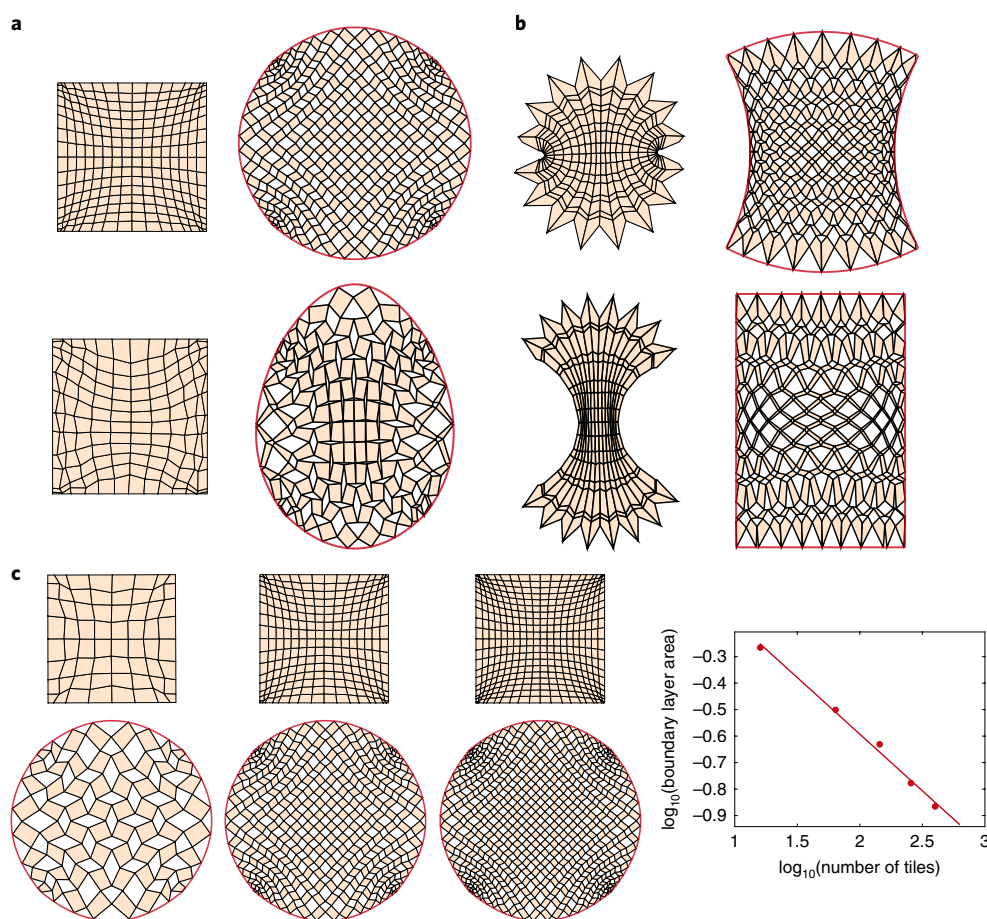


Fig. 2 | Generalized planar kirigami patterns. **a**, Examples of generalized kirigami patterns produced by our method for getting a circle or an egg shape from a square on deployment. **b**, Examples of generalized kirigami patterns produced by our method for achieving boundary shapes with mixed curvature or zero curvature. It can be observed that our method is capable of producing generalized kirigami patterns that match boundary curves with different curvature properties when deployed. **c**, Examples of circling the square with different resolutions (number of tiles = 8×8 , 16×16 , 20×20), together with a log–log plot of the boundary layer area against the number of tiles. Here, the boundary layer area is defined as the total area of the gaps between the circle and the boundary of the deployed kirigami patterns. The dots on the log–log plot represent kirigami patterns with different numbers of tiles (4×4 , 8×8 , 12×12 , 16×16 , 20×20) and the straight line is the least-square regression line. The result shows that there is an accuracy–effort trade-off in approximating a prescribed shape using generalized kirigami tessellations.

kirigami patterns with other base tessellations). These generalized kirigami patterns with different base tessellations exhibit different behaviours in terms of their effective porosity and overall magnification relative to their compact state (see Supplementary Information, Section 5). These examples naturally raise the question: what are the limits of kirigami design? One expects that these generalized kirigami patterns can only achieve a range of relative area changes, perimeter changes and curvature changes on deployment, and we can provide theorems on these bounds (see Supplementary Information, Section 6). However, since these bounds are a strong function of cut topology, it is possible, nevertheless, to generate a large variety of shapes.

Increasing the accuracy of the approximation using kirigami tessellations can be achieved by using a larger number of smaller tiles, suggesting that there is an accuracy–effort trade-off in matching a prescribed shape. Figure 2c shows several generalized kirigami patterns for circling the square with increasing accuracy; with more tiles, the boundary of the deployed pattern gets closer to a perfect circle (see Supplementary Information, Section 4 for multiresolution results for other patterns). To quantitatively assess the accuracy of the patterns for the approximation, we define the boundary layer area of a generalized kirigami pattern by the total area of the

gaps between the target boundary shape and the boundary of the deployed configuration. Figure 2c shows that the boundary layer area (denoted by A) decreases as the number of tiles (denoted by n^2) increases following the power law $A \propto (n^2)^{-1/2} = n^{-1}$. To further explain this, we approximate every boundary gap by a triangle and measure the change in the average triangle base length \bar{l} and average triangle height \bar{h} for different resolutions. We observe that $\bar{l} \propto n^{-1}$ and $\bar{h} \propto n^{-1}$, and hence the average area of the triangles $\bar{a} \propto n^{-2}$. As the number of boundary gap triangles is approximately $4n$, we have $A \approx 4n\bar{a} \propto n^{-1}$.

While our inverse design approach guarantees that the end-points of deployment, that is the deployed and undeformed states, exist, our method so far is agnostic to the path of deployment. To explore the deployment process of our patterns, we now extend our purely geometrical approach to a mechanical model by having linear springs along the edges and diagonals of the quads, and simple torsional springs at the nodal hinges to model the ligaments there. Then, the total mechanical energy of the system is given by

$$E(\mathbf{x}_1, \mathbf{x}_2, \dots, \mathbf{x}_N) = \frac{1}{N_s} \sum_{ij} \left(\frac{\|\mathbf{x}_i - \mathbf{x}_j\| - l_{ij}}{l_{ij}} \right)^2 + \lambda \frac{1}{N_c} \sum_i \theta_i^2 \quad (6)$$

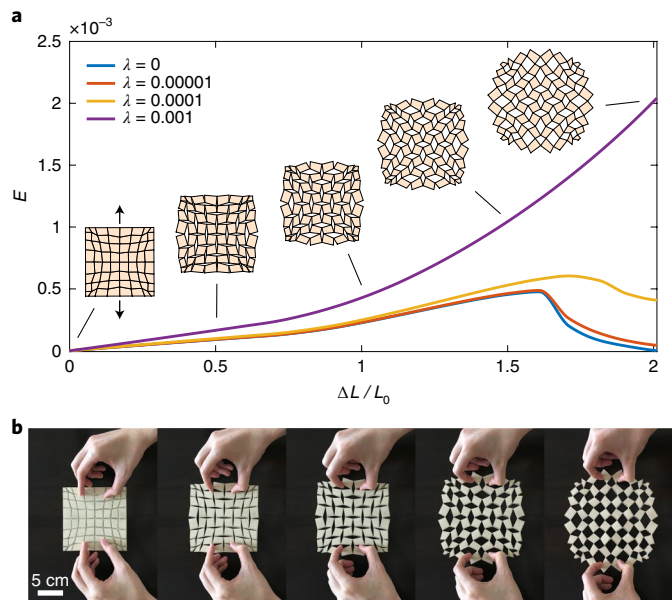


Fig. 3 | Planar deployment of generalized kirigami tessellation.

a, Energetics of the deployment simulations of the square to circle example with different choice of λ . Here ΔL is the average displacement of the pulling points and L_0 is the average rest length of the extensional springs. The insets show the initial, intermediate and final configurations of the generalized kirigami pattern under deployment. **b**, Snapshots of the deployment of a monostable fabricated model.

where \mathbf{x}_i are the locations of the nodes, θ_i are the angles between every pair of edges created under the cuts, l_{ij} are the rest lengths of the extensional springs, N_s is the total number of extensional springs, N_c is the total number of torsional springs and λ is the ratio of the torsional spring constant to the extensional spring constant. A larger λ corresponds to a thicker ligament, which has a stronger tendency to close up. By iteratively moving the boundary nodes towards the target boundary shape and solving for the intermediate deployed configurations by minimizing (6), we obtain a continuous deployment path. Figure 3a shows the energetics of the deployment simulations as a function of λ : as $\lambda \rightarrow 0$, we see the appearance of bistability, while for sufficiently large λ , monostability is observed.

To test our predictions experimentally, we fabricated a physical model by laser cutting a sheet of super-stretchable abrasion-resistant natural rubber. Figure 3b shows the deployment snapshots of a fabricated model with monostability, demonstrating that the simulated path and real deployment have similar behaviours (see Supplementary Information, Section 4 for another fabricated model of a generalized kagome kirigami pattern).

Our inverse design approach has so far focused on approximating planar shapes. However, we now show that it can be extended to fit surfaces in three dimensions as well, so that the undeployed pattern space is in \mathbb{R}^2 while the deployed space is in \mathbb{R}^3 . To fit a surface S in \mathbb{R}^3 , we replace the boundary shape matching constraints (3) by the surface matching constraints so that every node \mathbf{x}_i in the deployed configuration satisfies the condition

$$\|\mathbf{x}_i - \tilde{\mathbf{x}}_i\|^2 = 0 \quad (7)$$

where $\tilde{\mathbf{x}}_i$ is the projection of \mathbf{x}_i onto S and $\|\cdot\|$ is the Euclidean 2-norm. The extra constraints for controlling the boundary shape of the undeployed configuration in the planar case (analogous to equation (3)) can be directly extended to the surface fitting problem (see Supplementary Information, Section 7).

One can easily note that the contractibility constraints for surface fitting are the same as in equations (1) and (2). For the non-overlapping constraints, to prevent adjacent faces in the deployed configuration from overlapping with or intersecting each other, we replace the unit normal $\hat{\mathbf{n}}$ in equation (4) by the normal computed using one of the two faces. This implies that we must enforce the following inequality constraints for every pair of adjacent faces in the deployed configuration:

$$\langle (\mathbf{b} - \mathbf{a}) \times (\mathbf{c} - \mathbf{a}), (\mathbf{c} - \mathbf{a}) \times (\mathbf{d} - \mathbf{a}) \rangle \geq 0 \quad (8)$$

where \mathbf{a} , \mathbf{b} , \mathbf{c} and \mathbf{d} are the nodes of adjacent faces, so that $(\mathbf{b}, \mathbf{a}, \mathbf{c})$ form a positive (right-hand ordered) angle between the two faces and similarly $(\mathbf{c}, \mathbf{a}, \mathbf{d})$ also form a positive (right-hand ordered) angle.

In addition to the above constraints, we need to enforce the condition that the faces are planar so that the volume of the tetrahedron associated with each face F vanishes, corresponding to the planarity constraint:

$$\text{Volume}(F) = 0 \quad (9)$$

More explicitly, for quad tessellations the constraint becomes

$$\langle (\mathbf{b} - \mathbf{a}) \times (\mathbf{c} - \mathbf{a}), \mathbf{d} - \mathbf{a} \rangle = 0 \quad (10)$$

where \mathbf{a} , \mathbf{b} , \mathbf{c} and \mathbf{d} are the four points of the quad F (see Supplementary Information for generalizations to other base tessellations). We note that this condition, which is automatically satisfied for planar deployment, differentiates the three-dimensional deployment problem from the two-dimensional one.

Finally, to get smooth solutions, we extend the objective function (5) and the contraction process from our planar design approach to three-dimensional surface fitting. This allows us to determine a valid generalized kirigami pattern that can be deployed to approximate a prescribed surface in three dimensions by solving a constrained optimization problem using *fmincon* in MATLAB, with equations (1), (2) and (7)–(9) to be satisfied.

In Fig. 4 we show several generalized kirigami patterns that can be deployed to fit surfaces of varying complexity, such as those with monotonic positive and negative gauss curvature (Fig. 4a,b). Additionally, just as for planar deployments, we can impose extra boundary angle constraints to produce different pattern design effects such as using rectangular quad patterns that can be deployed to fit either a hyperbolic paraboloid as shown in Fig. 4a or an elliptic paraboloid as shown in Fig. 4b. Our approach also allows us to design surfaces with complex non-monotonic Gauss curvature, for example a periodic patch of an egg-carton shape (Fig. 4c) and a bivariate Gaussian (Fig. 4d). In all these examples, we see that our kirigami algorithm provides locally planar tessellations that approximately tile surfaces in \mathbb{R}^3 that have non-zero curvature in general. This suggests that the effective surface curvature of the holes between the piecewise planar tilings must be non-zero. To quantify this, we fit every hole in the deployed configurations of our generalized quad kirigami patterns by a bicubic Bézier surface, and compute the mean curvature and the Gaussian curvature of the interpolant (see Supplementary Information, Section 7 for the details); the rightmost columns in Fig. 4 show that the holes between the planar tilings are indeed curved.

To simulate the physical process of deployment, we extend the planar energetic model into three dimensions, with an additional planarity constraint enforced to ensure that all quads remain planar through the simulations. Figure 5a shows the deployment simulations with the four boundaries of a generalized kirigami pattern pulled towards the target positions for fitting a hyperbolic paraboloid. While the intermediate states are warped, the final

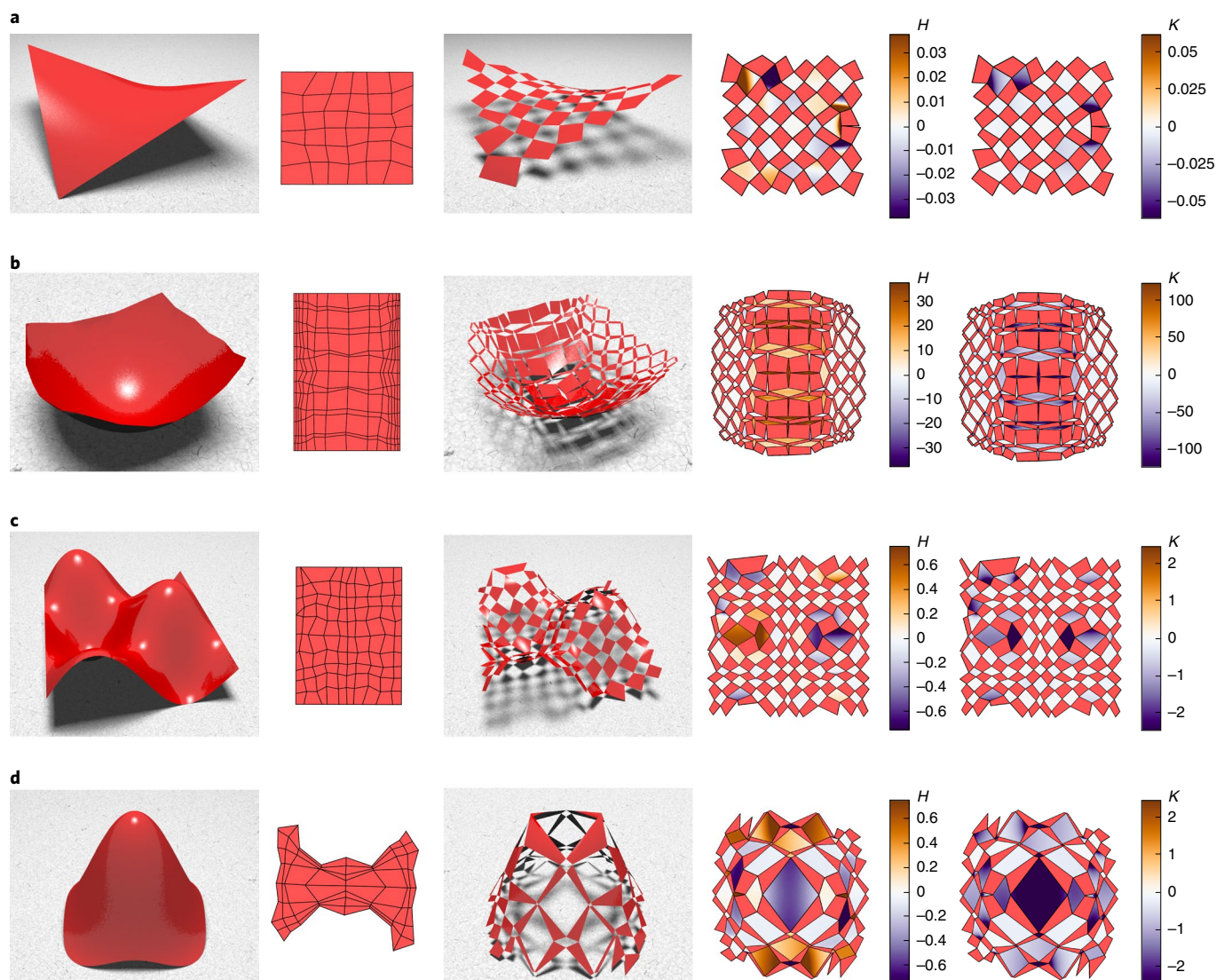


Fig. 4 | Generalized kirigami patterns for three-dimensional surface fitting. a–d. The target surfaces are a hyperbolic paraboloid (with negative curvature) (a), a paraboloid (with positive curvature) (b), a periodic patch of an egg-carton shape (c) and a bivariate Gaussian (d). Columns: the target surfaces (leftmost), the generalized kirigami patterns, the deployed configurations of the patterns that fit the target surfaces, the top views of the deployed patterns with the holes coloured with the approximated mean curvature H and the top views of the deployed patterns with the holes coloured with the approximated Gauss curvature K (rightmost).

deployed configuration resembles the shape of a smooth hyperbolic paraboloid very well. Furthermore, just as planar deployment can be either bistable or monostable depending on the value of the torsional spring constant λ , we see the same effect in three-dimensional deployment as well; when λ is large enough, the deployment becomes monostable.

Our inverse design framework is agnostic to the range of possible deployment trajectories aimed towards the target three-dimensional shape, for example by applying displacements to multiple parts of the boundary, as well as fabrication methods of physical kirigami structures. Figure 5b shows the manual deployment of a physical model of a hyperbolic paraboloid fabricated by laser cutting a natural rubber sheet model. We can also create generalized kirigami patterns by creating a mould into which one can pour a liquid polymer and cross-linking it (see Supplementary Information, Section 7 for a fabricated model produced using polydimethylsiloxane (PDMS) and generalized kagome kirigami patterns for surface fitting obtained by our method).

Our inverse design approach allows us to create non-periodic compact kirigami patterns that when deployed can approximate any given shape in two or three dimensions. Simple fabrication methods using cutting and moulding allow us to verify our designs for a few planar and three-dimensional deployable shapes. When our geometry-based constrained optimization framework is generalized to account for the mechanical response of the tilings and hinges, we see that the response of the generalized kirigami patterns can be tuned to switch between monostability and bistability. Altogether, harnessing the underlying topological and geometrical complexity of kirigami in a constrained optimization framework opens the path for the use of generalized kirigami tessellations as the building blocks of shape-morphing mechanical metamaterials. Simultaneously, the present work on inverse design of kirigami together with our ability to solve the inverse design problem in origami²² suggests a follow-up question: can we combine origami and kirigami, coupling geometry, topology and mechanics, to create structures that morph from any shape

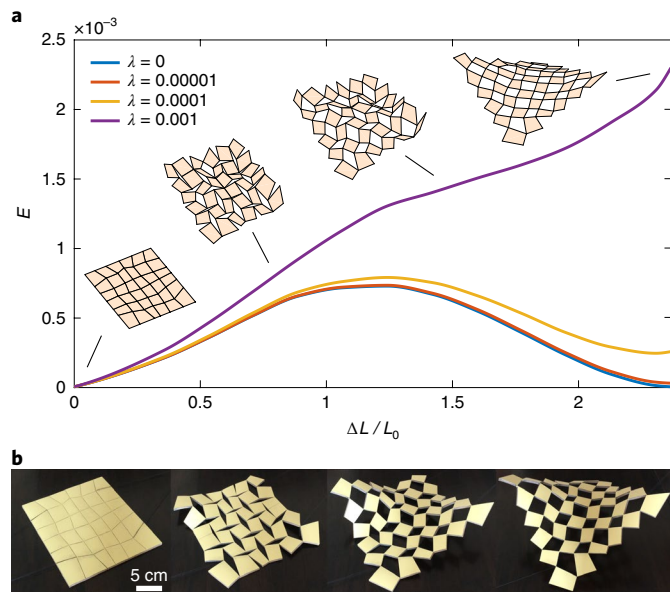


Fig. 5 | Three-dimensional deployment of generalized kirigami tessellation. **a**, Energetics of the three-dimensional deployment simulations of the pattern in Fig. 4a with different choices of λ . Here ΔL is the average displacement of the pulling points and L_0 is the average rest length of the extensional springs. The insets show the initial, intermediate and final configurations of the pattern under deployment. **b**, Snapshots of the deployment of a monostable fabricated model, with thin threads used for pulling the four sides. Both the numerical simulation and physical deployment results fit the hyperbolic paraboloid very well.

to a given shape with a given mechanical response in two or three dimensions?

Online content

Any methods, additional references, Nature Research reporting summaries, source data, statements of code and data availability and associated accession codes are available at <https://doi.org/10.1038/s41563-019-0452-y>.

Received: 24 October 2018; Accepted: 4 July 2019;
Published online: 19 August 2019

References

- Grima, J. N. & Evans, K. E. Auxetic behavior from rotating squares. *J. Mater. Sci. Lett.* **19**, 1563–1565 (2000).
- Grima, J. N., Alderson, A. & Evans, K. E. Negative Poisson's ratios from rotating rectangles. *Comp. Methods Sci. Technol.* **10**, 137–145 (2004).
- Grima, J. N., Alderson, A. & Evans, K. E. Auxetic behaviour from rotating rigid units. *Phys. Status Solidi B* **242**, 561–575 (2005).
- Rafsanjani, A. & Pasini, D. Bistable auxetic mechanical metamaterials inspired by ancient geometric motifs. *Extreme Mech. Lett.* **9**, 291–296 (2016).
- Sussman, D. M. et al. Algorithmic lattice kirigami: a route to pluripotent materials. *Proc. Natl Acad. Sci. USA* **112**, 7449–7453 (2013).

- Blees, M. K. et al. Graphene kirigami. *Nature* **524**, 204–207 (2015).
- Zhang, Y. et al. A mechanically driven form of Kirigami as a route to 3D mesostructures in micro/nanomembranes. *Proc. Natl Acad. Sci. USA* **112**, 11757–11764 (2015).
- Shyu, T. C. et al. A kirigami approach to engineering elasticity in nanocomposites through patterned defects. *Nat. Mater.* **14**, 785 (2015).
- Rafsanjani, A. & Bertoldi, K. Buckling-induced kirigami. *Phys. Rev. Lett.* **118**, 084301 (2017).
- Konaković, M. et al. Beyond developable: computational design and fabrication with auxetic materials. *ACM Trans. Graph.* **35**, 89 (2016).
- Tang, Y. & Yin, J. Design of cut unit geometry in hierarchical kirigami-based auxetic metamaterials for high stretchability and compressibility. *Extreme Mech. Lett.* **12**, 77–85 (2017).
- Gatt, R. et al. Hierarchical auxetic mechanical metamaterials. *Sci. Rep.* **5**, 8395 (2015).
- Kolken, H. M. & Zadpoor, A. A. Auxetic mechanical metamaterials. *RSC Adv.* **7**, 5111–5129 (2017).
- Mitschke, H., Robins, V., Mecke, K. & Schröder-Turk, G. E. Finite auxetic deformations of plane tessellations. *Proc. R. Soc. Lond. A* **469**, 20120465 (2013).
- Shan, S., Kang, S. H., Zhao, Z., Fang, L. & Bertoldi, K. Design of planar isotropic negative Poisson's ratio structures. *Extreme Mech. Lett.* **4**, 96–102 (2015).
- Isobe, M. & Okumura, K. Initial rigid response and softening transition of highly stretchable kirigami sheet materials. *Sci. Rep.* **6**, 24758 (2016).
- Neville, R. M., Scarpa, F. & Pirrera, A. Shape morphing kirigami mechanical metamaterials. *Sci. Rep.* **6**, 31067 (2016).
- Celli, P. et al. Shape-morphing architected sheets with non-periodic cut patterns. *Soft Matter* **14**, 9744–9749 (2018).
- Grünbaum, B. & Shephard, G. C. *Tilings and Patterns* (Freeman, 1987).
- Choi, G. P.-T. & Lui, L. M. A linear formulation for disk conformal parameterization of simply-connected open surfaces. *Adv. Comput. Math.* **44**, 87–114 (2018).
- Meng, T. W., Choi, G. P.-T. & Lui, L. M. TEMPO: feature-endowed Teichmüller extremal mappings of point clouds. *SIAM J. Imaging Sci.* **9**, 1922–1962 (2016).
- Dudte, L. H., Vouga, E., Tachi, T. & Mahadevan, L. Programming curvature using origami tessellations. *Nat. Mater.* **15**, 583–588 (2016).

Acknowledgements

This work was supported in part by the Croucher Foundation (G.P.T.C.), National Science Foundation grant no. DMR 14-20570 (L.M.), DMREF grant no. 15-33985 (L.M.) and EFRI grant no. 18-30901 (L.M.). We thank M. Goldberg for contributing to preliminary numerical work, M. Gazzola for helpful initial discussions, and A. Nagarkar and the Whitesides Group for help with fabrication of some of the models using PDMS.

Author contributions

L.H.D. and L.M. conceived the research. G.P.T.C., L.H.D. and L.M. designed the research. G.P.T.C. and L.H.D. conducted the simulations and built the models. G.P.T.C., L.H.D. and L.M. analysed the results and wrote the manuscript.

Competing interests

We have filed a patent on our algorithms for kirigami design.

Additional information

Supplementary information is available for this paper at <https://doi.org/10.1038/s41563-019-0452-y>.

Reprints and permissions information is available at www.nature.com/reprints.

Correspondence and requests for materials should be addressed to L.M.

Publisher's note: Springer Nature remains neutral with regard to jurisdictional claims in published maps and institutional affiliations.

© The Author(s), under exclusive licence to Springer Nature Limited 2019

Methods

Experiment. The physical models shown in Figs. 3 and 5 were fabricated by perforating patterns on super-stretchable abrasion-resistant natural rubber sheets with a laser cutter. See Supplementary Information for further details and another physical model fabricated using PDMS.

Numerical computations. The numerical computations (solving the constrained optimization problem and analysing energetics) were conducted with custom MATLAB code. Analytic gradients of the constraints and objective functions are provided to the *fmincon* constrained optimization routine within the MATLAB

environment. See Supplementary Information for further details on the constraints, objective functions and initial conditions.

Data availability

The data that support the findings of this study are available from the corresponding author on reasonable request.

Code availability

Computer codes used in this study are available from the corresponding author on request.